PHYSICAL REVIEW B **95**, 161405(R) (2017)

Ballistic and resonant negative photocurrents in semiconducting carbon nanotubes

Christoph Karnetzky,[1,2] Lukas Sponfeldner,[1] Max Engl,[1] and Alexander W. Holleitner[1,2,*]

[1]*Walter Schottky Institute and Physics Department, Technical University Munich, Am Coulombwall 4(a), 85748 Garching, Germany*

[2]*Nanosystems Initiative Munich (NIM), Schellingstrasse 4, 80799 Munich, Germany*

(Received 1 November 2016; revised manuscript received 17 February 2017; published 12 April 2017)

Ultrafast photocurrent experiments are performed on semiconducting, single-walled carbon nanotubes under a resonant optical excitation of their subbands. The photogenerated excitons are dissociated at large electric fields and the resulting transport of the charge carriers turns out to be ballistic. Thermionic emission processes to the contacts dominate the photocurrent amplitude. The charge current without laser excitation is well described by a Fowler-Nordheim tunneling. The time-averaged photocurrent changes polarity as soon as sufficient charge carriers are injected from the contacts, which can be explained by an effective population inversion in the optically pumped subbands.

DOI: 10.1103/PhysRevB.95.161405

Carbon nanotubes (CNTs) exhibit one-dimensional electron systems with a large exciton binding energy of several hundreds of meV [1,2] and they allow for the fundamental investigation of exciton- and electron-phonon interactions in reduced dimensions [3–5]. Despite the large exciton binding energy, the generation of a photocurrent has been reported in several experiments [6,7]. It is largely discussed in terms of photothermoelectric effects in combination with electric fields induced by potential fluctuations and contact potentials [7–14]. However, there is still very little known about the temporal dynamics of the charge transport to the contacting reservoirs with regard to the exciton dissociation as well as the relaxation and recombination dynamics within the CNTs' subbands. Recent work on *p-i-n* junctions in CNTs reveals a diffusive transport of photogenerated charge carriers to the contacts with an onset of ballistic transport at high electric fields [15]. For unbiased CNTs, further work introduces a "spontaneous dissociation" of excitons giving rise to a photocurrent, without clarifying the underlying transport processes [16]. Moreover, it is unclear whether the mechanism of the photoinduced nonequilibrium charge transport can be distinct to the charge transport without laser excitation.

We reveal the ultrafast, nonequilibrium transport properties of photogenerated electrons and holes in few to single semiconducting CNTs. We compare the results for CNTs where either the second or first subband is resonantly excited. We demonstrate that the ultrafast photocurrent in the CNTs is dominated by a ballistic transport. By a time-of-flight analysis, we resolve a ballistic group velocity of the photogenerated charge carriers. Moreover, we identify a thermionic emission of the photogenerated charge carriers to the contacts. In this picture, photogenerated charge carriers with a high kinetic energy can overcome the energy barriers to the contacts, and they drive the overall photocurrent. The mechanism stands in contrast to the process which we find for the so-called dark current, i.e., the charge transport without laser excitation. Here, a Fowler-Nordheim tunneling of charge carriers from the contacts to the CNTs consistently describes the data. The overall slowest optoelectronic processes occur on a nanosecond time scale. We detect them at very high bias voltages, and they are consistent with a so-called lifetime-limited photocurrent, as recently reported for ensembles of CNTs [17]. In time-averaged measurements, we observe a sign change of the photocurrent for a high bias, which we explain by an effective population inversion of the optically pumped subband of the CNTs via charge tunneling processes from the metal contacts. Our experiments give fundamental insights into the ultrafast dynamics of photogenerated charge carriers in contacted, semiconducting CNTs ranging from the photocurrent generation to the nonequilibrium transport of the charges to and from the contacts. The insights may prove essential for ultrafast optoelectronic devices and photodetectors based on semiconducting CNTs in general, but particularly on single CNTs integrated into optoelectronic high-speed circuits and THz striplines.

The experiments are performed on two sets of semiconducting CNTs. The first is synthesized by the arc-discharge method and the second by cobalt-molybdenum catalyst based synthesis [18–20]. The first (second) CNTs have a diameter of $d_{\mathrm{CNTS}} \sim 1.5\,\mathrm{nm}$ (0.8 nm). Via dielectrophoresis [21], the CNTs are deposited in between two Ti/Au contacts with a height of 10/300 nm [Fig. 1(a)]. The contacts are fabricated by optical lithography and they form lateral, coplanar striplines with a total length of ∼58 mm, a width of 5 μm, and a separation of 10 μm. The striplines are utilized to perform the ultrafast, time-resolved photocurrent experiments [22–25]. At the position of the CNTs, the distance between the striplines is reduced to 1.1–0.1 μm. All measurements are performed at $\sim 10^{-6}$ mbar and 77 K in a cryostat. We use a fiber-based pulsed laser with a pulse duration of <30 fs, a photon energy continuum between 0.9 and 1.3 eV, and a repetition frequency of 80 MHz. For measuring the time-integrated photocurrent I_{photo}, the photon energy E_{photon} is further filtered by using a monochromator such that the laser power P_{laser} amounts to $\sim 100\,\mathrm{W/cm^2}$ on the CNTs per center wavelength. We confirm the positioning of few to single CNTs between the contacts by using a scanning photocurrent microscopy with a lateral resolution of about 2 μm [Fig. 1(b)]. Figure 1(c) shows the photocurrent spectrum of I_{photo} vs E_{photon} measured at the position in between the two metal contacts. For all applied bias voltages V_{sd}, the photocurrent exhibits a clear maximum at $E_{\mathrm{photon}} \sim 1.15\,\mathrm{eV}$. This energy coincidences with the anticipated transition energy $E_{22} = C_2 - V_2$ between

*holleitner@wsi.tum.de

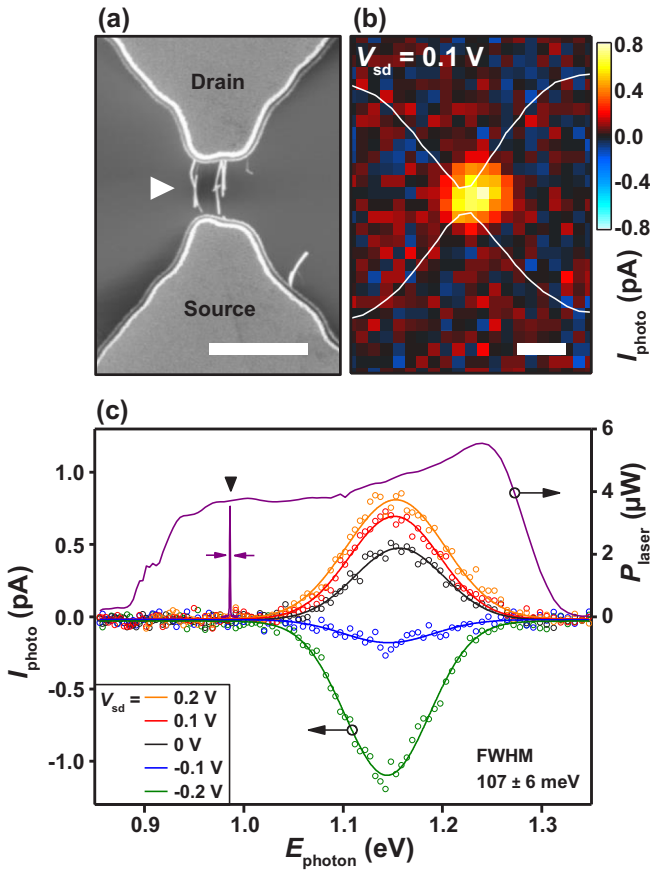

FIG. 1. (a) Scanning electron microscopy (SEM) image of metal contacts and single CNTs with $d_{CNTS} \sim 1.5$ nm (white triangle). (b) Time-integrated photocurrent I_{photo} vs spatial coordinates at $E_{photon} = 1.15$ eV. White lines indicate the edges of metal contacts. Scale bars are 2 μm. (c) Photocurrent I_{photo} vs E_{photon} at the position of the maximum in (b). The dashed line shows the excitation spectrum of the broadband laser. The bold triangle highlights the scanned energy window of the monochromator used.

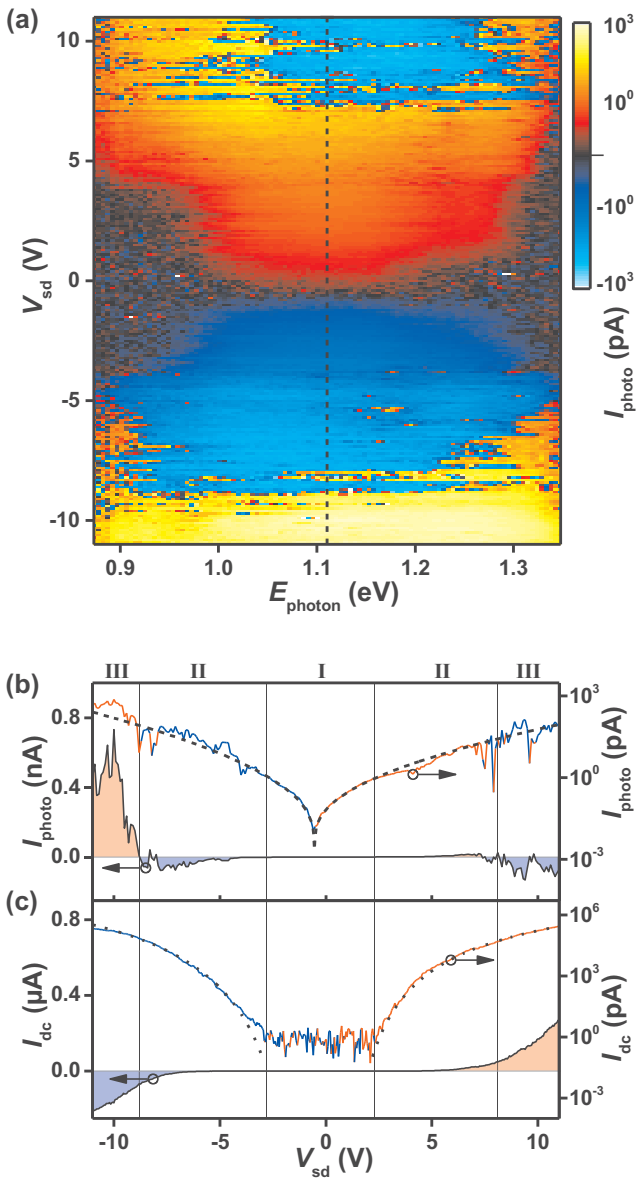

FIG. 2. (a) I_{photo} vs E_{photon} and V_{sd} as a logarithmic color plot for CNTs with $d_{CNTS} \sim 1.5$ nm. (b) Cross section along the dashed line at $E_{photon} = 1.15$ eV in (a) in linear and logarithmic scale. Red (blue) color indicates the positive (negative) sign of I_{photo}. (c) Dark current I_{dc} vs V_{sd} without laser excitation in linear and logarithmic scale. Dashed and dotted lines are fits to the data. The regimes I, II, and III are defined in the text.

the second conduction (valence) band C_2 (V_2) for the given diameter $d_{CNTS} \sim 1.5$ nm of the discussed CNTs [26]. The full width at half maximum FWHM $= 107 \pm 6$ meV compares reasonably well with reported values [7,12,14,15,16]. However, we cannot exclude intra-CNT charge carrier dynamics or different species of CNTs because of the chosen fabrication method [20,21]. Figure 1(c) already demonstrates that a photocurrent is measured even at zero bias and for voltages much smaller than the exciton binding energy.

Figure 2(a) shows a false-color plot of the time-integrated photocurrent I_{photo} vs E_{photon} and V_{sd}. For $|V_{sd}| \geqslant 8$ V, we observe a sign change of I_{photo} which is clearly seen in the line scans I_{photo} vs V_{sd} for a fixed photon energy [$E_{photon} = 1.15$ eV in Fig. 2(b)]. The dashed line in Fig. 2(b) describes a thermionic emission process with barrier lowering, i.e., Schottky emission of photogenerated charge carriers from the CNTs across the contact barriers into the metal contacts [20]. Interestingly, also in the high voltage regime where I_{photo} changes sign, the amplitude of I_{photo} follows this thermionic model. For comparison, Fig. 2(c) shows the dark current I_{dc} without laser illumination for the same bias regime. We observe that I_{dc} does not show a sign change and that the data can be fitted by a Fowler-Nordheim tunneling [dotted line in Fig. 2(c)]. Considering the voltage dependences of I_{photo} and I_{dc}, we identify three voltage regimes I, II, and III for CNTs, in which the second subband is resonantly excited. In regime I, $|V_{sd}| \leqslant 2.5$ V, no I_{dc} passes through the sample, while a laser excitation leads to photogenerated charge carriers and hence to a finite I_{photo}. In regime II, 2.5 V $\leqslant |V_{sd}| \leqslant 8$ V, a finite I_{dc} can be measured in addition to I_{photo}. In regime III, $|V_{sd}| \geqslant 8$ V, I_{photo} changes sign while the sign change does not occur for I_{dc}. We note that for regime III, the amplitude of I_{photo} is about

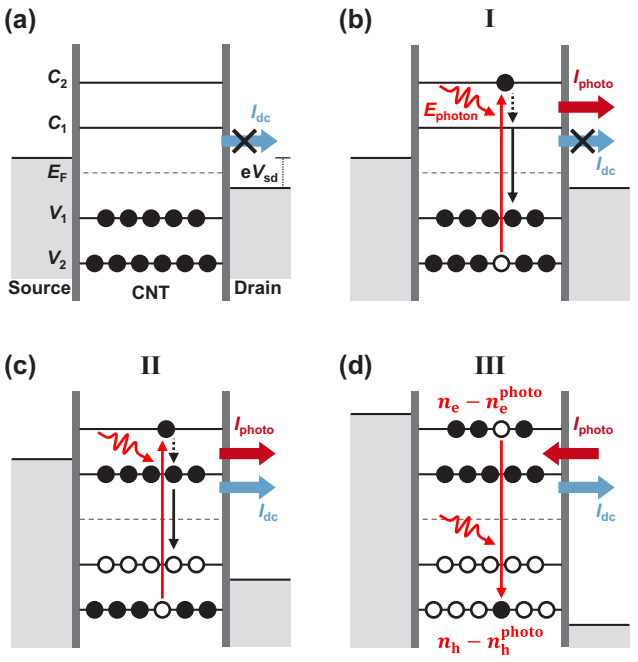

FIG. 3. Sketched band diagram of CNTs for the three voltage regimes I, II, and III. For simplicity, contact barriers are schematically depicted as thick vertical lines. (a) V_{sd} in regime I without laser excitation. (b)–(d) V_{sd} in regimes I–III including the laser excitation. See text for details.

three orders of magnitude smaller than the amplitude of I_{dc}. In this respect, the measured I_{photo} can be understood as a small modulation of I_{dc} by the laser excitation.

Figure 3 sketches the band structure of the contacted CNTs excited at the second subbands. For clarity, we discuss only the dynamics for electrons, since the hole dynamics is symmetric in energy. In regime I and no laser excitation [Fig. 3(a)], we can neglect I_{dc} as the thermal activation energy $k_B T \sim 7$ meV is too small for the electrons to be emitted from the metal contacts into the conduction subbands C_1 (C_2) and from the valence subbands V_1 (V_2) to the contacts. In regime I with a laser excitation resonant to E_{22}, electrons are optically excited from V_2 to C_2 [upward arrow in Fig. 3(b)]. Then, they relax and recombine within the CNTs (dotted and black downward arrows) and/or they propagate to the contacts (arrow to the right). The corresponding overall photocurrent can be described as

$$I_{photo} = n_e^{photo} e v, \tag{1}$$

with n_e^{photo} an effective density of photogenerated electrons in the CNTs, v their average velocity, and e the elementary charge. We observe a finite I_{photo} at no I_{dc} in this regime, which further suggests that the electron transfer from the subbands to the contacts occurs on a similar time scale as the relaxation and recombination processes within the CNTs, i.e., on femtoseconds to picoseconds [27]. This nonequilibrium scenario explains that I_{photo} can be described by a thermionic emission model, as expected for photogenerated charge carriers with a high kinetic energy. In regime II [Fig. 3(c)], electrons from the metal contacts can tunnel into the first subband of the CNTs, generating the current I_{dc} as detected in our measurement without laser excitation [Fig. 2(c)]. Consistently, we can describe I_{dc} by a Fowler-Nordheim tunneling process, which sets in at a finite bias voltage [20]. We note that this current is not detected in the signal I_{photo} [Fig. 2(b)], since it is not coherent with respect to the chopper reference. I_{photo} is still well described by the thermionic model in this regime. Furthermore, electrons in V_1 can tunnel into the drain contact, such that this subband can be assumed to have empty states available [Fig. 3(c)]. In regime III [Fig. 3(d)], electrons from the metal contacts can now also tunnel into C_2, where they can interact with the laser excitation. Moreover, electrons both in V_1 and V_2 can quickly tunnel to the drain contact, such that, on average, both subbands have free electron states available. Overall, this scenario leads to a population inversion. Because of the conduction and valence band symmetry in CNTs, the rate for an optical transition from C_2 to V_2 equals the one from V_2 to C_2 which can be assumed to be on a subpicosecond time scale [28]. Hence, the optical transition C_2 to V_2 occurs on a time scale comparable to the time scales of internal relaxation and recombination processes [27]. This stimulated emission then reduces the overall electron density n_e in C_2 by an amount of $-n_e^{photo}$. The corresponding reduction of I_{dc} has the opposite sign to I_{dc}, and it is coherent to the chopper reference. Therefore, it shows up in the signal I_{photo} with a negative sign. In terms of Eq. (1), I_{photo} can be written as $-n_e^{photo} e v$. Hereby, we explain the sign change of I_{photo} in regime III [Fig. 2(b)]. The arguments equally apply to the hole states in the CNTs because of the mentioned electron-hole symmetry.

In principle, Fig. 3 assumes that only single CNTs carry the (photo)current without any intertube contacts in between the two metal reservoirs. However, the figure summarizes our present understanding to explain the experimental data of Figs. 1 and 2, including the polarity change of I_{photo} and that I_{dc} is below the noise level in regime I. Alternative processes, such as optical gating, would rather change the Fermi level and therefore the amplitude of I_{photo} [29]. This is a different scenario than our results in Fig. 2(b), where the dashed line nicely describes the absolute value of I_{photo}, although its polarity switches. Furthermore, all measurements are carried out in vacuum, such that we can neglect a scenario such as photodesorption [29]. A photogating via the substrate is also improbable because the reported polarity change depends reproducibly on the bias voltage [cf. Fig. 2(b)].

The discussed sequence of regimes I, II, and III is generic to semiconducting CNTs which are resonantly excited in the second subbands. We find an equivalent sign change of the photocurrent, when we resonantly pump the first subbands. This experiment has been performed on the second set of CNTs with $d_{CNTS} \sim 0.8$ nm [20]. We note that in all cases the values of the applied bias voltages for the different regimes are determined mainly by the contact morphology. They do not necessarily correspond to the subband energy spacings within the CNTs [30].

In order to resolve the underlying nonequilibrium dynamics within the CNTs, we perform time-resolved ultrafast photocurrent measurements (again shown for the first set of CNTs with $d_{CNTS} \sim 1.5$ nm). We use an on-chip THz-time domain

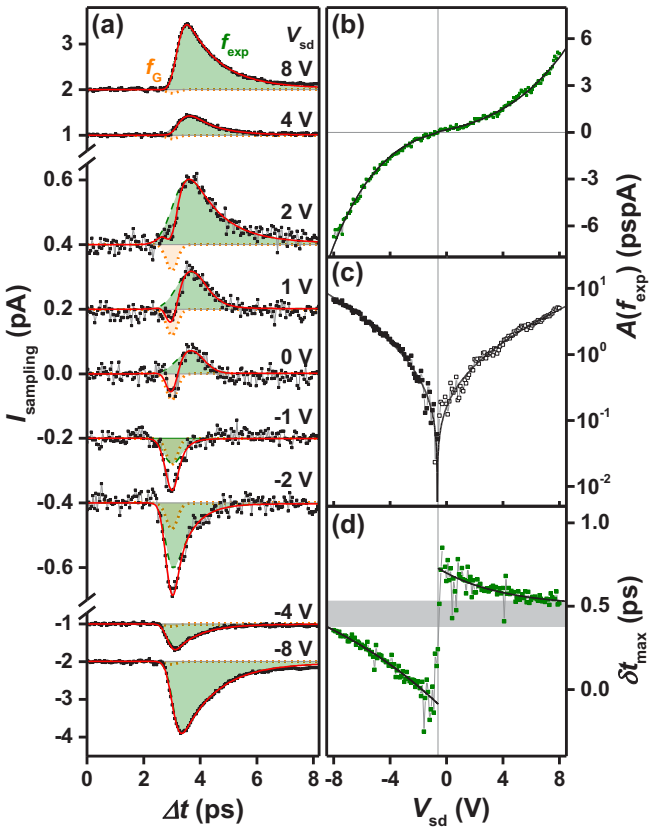

FIG. 4. (a) Time-resolved photocurrent $I_{sampling}$ vs Δt for different V_{sd} for CNTs with $d_{CNTS} \sim 1.5$ nm. The red line is the sum of a Gaussian f_G (dotted orange line) and an exponential decay f_{exp} (dashed green line). (b) Fit area $A(f_{exp})$ vs V_{sd}. (c) Logarithmic plot of $A(f_{exp})$. (d) Relative time delay δt between f_G and f_{exp} as a function of V_{sd}.

photocurrent spectroscopy where the femtosecond pump laser excites the electronic states within the CNTs. This laser is the same as for I_{photo} in Fig. 2. Since the contacts form striplines, the photocurrent also gives rise to electromagnetic transients in the metal striplines with a bandwidth of up to 2 THz [22–25]. In particular, the odd mode of the striplines is utilized to trigger transients in the high-frequency circuits [31]. The transients run along the striplines, and they are detected on chip by a time-delayed optical femtosecond probe pulse in combination with an Auston switch [22]. We use ion-implanted amorphous silicon for this ultrafast photodetector with a subpicosecond time resolution [23,24]. The current $I_{sampling}$ across the Auston switch is sampled as a function of the time delay Δt between the two laser pulses, and it is directly proportional to the ultrafast photocurrents in the CNTs [17].

Figure 4(a) shows $I_{sampling}$ vs Δt for varying V_{sd}. We fit $I_{sampling}(\Delta t)$ with two functions. The first is a Gaussian f_G having a FWHM $= 460 \pm 10$ fs (dotted line). It describes the ultrafast displacement current at the CNT-Au contact of the stripline circuit [17], which defines the moment of time when the laser pulse impinges onto the striplines with respect to the propagation of the photogenerated charge carriers in the CNTs. The FWHM of f_G is determined by the effective dispersion and attenuation of the THz circuit. The second fit component is a Gaussian convoluted decay function f_{exp} with a decay time τ_1 (dashed lines). Figures 4(b) and 4(c) depict the area $A(f_{exp})$ vs V_{sd} in a linear and logarithmic scale, respectively. Again, $A(f_{exp})$ can be consistently fitted by a thermionic emission process [black lines in Figs. 4(b) and 4(c) and dashed lines in Fig. 2(b)] [20]. In our interpretation, these are the photogenerated charge carriers with an energy high enough to overcome the contact barriers, which also dominate the time-averaged signal I_{photo}. Interestingly, the relative time delay δt of the photocurrent within the CNTs (f_{exp}) with respect to the displacement peak (f_G) varies for positive and negative V_{sd} [Fig. 4(d)]. In particular, for a positive V_{sd} approaching zero bias, δt reaches 0.8 ± 0.1 ps. For a negative V_{sd} approaching zero bias, δt reaches zero. This asymmetry suggests that the photocurrents are generated at the two contacts. With a distance of 1.1 ± 0.1 μm between the two contacts, we compute a velocity $(1.1–1.6)\times10^6$ ms^{-1}. Within the errors, this velocity agrees well with the ballistic group velocity of the CNTs [32], and it is significantly below a plasmon velocity [33,34]. The interpretation of a ballistic transport is further corroborated by the variation of δt for large V_{sd} [Fig. 4(d)]. There, for both polarities of V_{sd}, δt reaches values of 0.4–0.5 ps (gray area). We argue that at large bias, the voltage drops across the whole length of the CNTs while the contact barriers become transparent, and, in turn, excitons can be dissociated along the center part of the CNTs as well. Since the laser spot exceeds the length of the CNTs, $I_{sampling}$ senses the center motion of all photogenerated charge carriers along half the length of the CNT in average. Accordingly, we calculate an average propagation velocity of $\frac{1}{2}(1.1 \pm 0.1)$ μm/(0.4–0.5) ps $= (1.0–1.5)\times10^6$ ms^{-1}, which again agrees well with an anticipated ballistic group velocity. The interpretation of a ballistic propagation is substantiated by three facts. First, the deduced velocities exceed typical values for a drift saturation velocity of 5×10^5 ms^{-1} [3]. Second, we detect a similar propagation velocity for the second set of CNTs where only the first subband is excited and solely participating in the nonequilibrium transport [20]. This is in agreement with recent estimations on the ballistic group velocity based on zone folding arguments [32]. Third, the effective mass in the first subband is about two times smaller than in the second subband. A diffusive transport of single-particle excitations would give a correspondingly shorter escape time and therefore an increased apparent transport velocity [15]. Although we cannot perform a comparative study on the velocities in the first and second subband within one kind of CNT (because of laser limitations), the deduced values at zero and finite bias are already at the upper limit of a ballistic group velocity in CNTs for both sets of CNTs. Moreover, our findings at zero and large bias in Fig. 4(d) clearly indicate that the photogenerated excitons are dissociated at high electric fields, i.e., at contact potentials and at an applied bias. We propose that the dissociation of the resonantly photogenerated excitons in both the first and second subbands releases enough energy such that the electrons and holes propagate ballistically at a large kinetic energy. These are the charge carriers which show up as a thermionic current [Figs. 2(b) and 4(c)]. In principle, the length of 1.1 ± 0.1 μm exceeds the typical scattering length of high-energy optical phonons of about 100 nm [35]. However, it was recently demonstrated that photogenerated charge carriers in C_2

(and V_2) relax within the CNTs to C_1 (and V_1) within a few hundreds of femtoseconds most likely via TO phonons [27]. As a result, C_1 and V_1 fill up with hot charge carriers also at finite k vectors, and the cooling of the electron baths in C_1 and V_1 then occurs via longitudinal acoustic (LA) phonons on a time scale of a few picoseconds [27]. In our interpretation, the peak value of I_{sampling} comprises the fasted (ballistic) ensembles of such hot charge carriers in C_1 and V_1. Consistent with this interpretation, the mean free path for a LA-phonon dominated transport is reported to be as long as micrometers at comparable low temperatures [36]. Yet, we note that it is difficult to directly compare our ultrafast nonequilibrium experiment to transport studies with thermalized electron and phonon baths in equilibrium. Within the above interpretation, we explain the decay time τ_1 of f_{exp} to represent the relaxation and cooling of the electron bath (in C_1 and V_1) of the CNTs in combination with a slower diffusive/drift transport regime. For large biases, τ_1 reaches values of 1.1–1.3 ps, while it is indistinguishable from the FWHM of f_{G} close to zero bias. The found values of τ_1 are consistent with the relaxation dynamics found in pure optical pump-probe studies on HiPco CNTs, which were equally excited in the second subbands and similarly treated with chemicals before [27].

We note that we do not observe a sign change of f_{exp} for the highest V_{sd} as we do for the time integrated [regime III in Fig. 2(b)]. This can be explained by the utilized ultrafast measurement technique. In the THz-time domain photocurrent spectroscopy, we do not measure the charge current directly. Instead, we probe the photoinduced electric field change. Due to the symmetric band structure of CNTs, photogenerated electrons and holes induce the same electric field. Hereby, the sign change does not show up in the I_{sampling}. We point out that at high bias voltages, an additional decay time with $\tau_2 = 1.2 \pm 0.7$ ns shows up [20]. We interpret the latter as the lifetime of the photogenerated charge carriers, as has been demonstrated for ensembles of CNTs [17]. Finally, we note that a Fermi-level tuning of the CNTs would require nanoscale split gates below the CNTs with the design challenge not to short circuit the high-frequency response of the on-chip THz circuit [37].

To conclude, we reveal the photocurrent generation and dynamics in semiconducting carbon nanotubes which are resonantly excited by a laser field. We find clear evidence that the photogenerated excitons are dissociated by electric fields at the contacts and within the CNTs at high biases. In a time-of-flight analysis, we extract a ballistic group velocity of the fasted photogenerated charge carriers. The dark current without laser excitation can be described by a Fowler-Nordheim tunneling. Moreover, we find that the photocurrent changes polarity as soon as the resonantly pumped subband is populated by charge carriers from the contact.

We thank the European Research Council (ERC) for financial support via project “NanoREAL” (No. 306754).

[1] F. Wang, G. Dukovic, L. E. Brus, and T. F. Heinz, Science **308**, 838 (2005).
[2] J. Maultzsch, R. Pomraenke, S. Reich, E. Chang, D. Prezzi, A. Ruini, E. Molinari, M. S. Strano, C. Thomsen, and C. Lienau, Phys. Rev. B **72**, 241402(R) (2005).
[3] V. Perebeinos, J. Tersoff, and P. Avouris, Phys. Rev. Lett. **94**, 086802 (2005).
[4] A. Hartschuh, E. J. Sánchez, X. S. Xie, and L. Novotny, Phys. Rev. Lett. **90**, 095503 (2003).
[5] T. Hertel and G. Moos, Phys. Rev. Lett. **84**, 5002 (2000).
[6] A. Fujiwara, Y. Matsuoka, H. Suematsu, N. Ogawa, K. Miyanoi, H. Kataura, Y. Maniwa, S. Suzuku, and Y. Achiba, Jpn. J. Appl. Phys. **40**, L1229 (2001).
[7] M. Freitag, Y. Martin, J. A. Misewich, and P. Avouris, Nano Lett. **3**, 1067 (2003).
[8] K. Balasubramanian, M. Burghard, K. Kern, M. Scolari, and A. Mews, Nano Lett. **5**, 507 (2005).
[9] M. Freitag, J. C. Tsang, A. Bol, D. Yuan, J. Liu, and P. Avouris, Nano Lett. **7**, 2037 (2007).
[10] Y. H. Ahn, A. W. Tsen, B. Kim, Y. W. Park, and J. Park, Nano Lett. **7**, 3320 (2007).
[11] P. Avouris, M. Freitag, and V. Perebeinos, Nat. Photon. **2**, 341 (2008).
[12] A. D. Mohite, P. Gopinath, H. M. Shah, and B. W. Alphenaar, Nano Lett. **8**, 142 (2008).
[13] N. Rauhut, M. Engel, M. Steiner, R. Krupke, P. Avouris, and A. Hartschuh, ACS Nano **6**, 6416 (2012).
[14] M. Barkelid and V. Zwiller, Nat. Photon. **8**, 47 (2014).
[15] N. M. Gabor, Z. Zhong, K. Bosnick, and P. L. McEuen, Phys. Rev. Lett. **108**, 087404 (2012).
[16] Y. Kumamoto, M. Yoshida, A. Ishii, A. Yokoyama, T. Shimada, and Y. K. Kato, Phys. Rev. Lett. **112**, 117401 (2014).
[17] L. Prechtel, L. Song, S. Manus, D. Schuh, W. Wegscheider, and A. W. Holleitner, Nano Lett. **11**, 269 (2011).
[18] IsoNanotubes-S, 98% from NanoIntegris, Inc.
[19] Enriched (6,5) CNTs (SG65i) from Chasm Technologies, Inc.
[20] See Supplemental Material at http://link.aps.org/supplemental/10.1103/PhysRevB.95.161405 for further details.
[21] A. Vijayaraghavan, S. Blatt, D. Weissenberger, M. Oron-Carl, F. Hennrich, D. Gerthsen, H. Hahn, and R. Krupke, Nano Lett. **7**, 1556 (2007).
[22] D. Auston, IEEE J. Quantum Electron. **19**, 639 (1983).
[23] A. Brenneis, L. Gaudreau, M. Seifert, H. Karl, M. S. Brandt, H. Huebl, J. A. Garrido, F. H. L. Koppens, and A. W. Holleitner, Nat. Nanotechnol. **10**, 135 (2015).
[24] C. Kastl, C. Karnetzky, H. Karl, and A. W. Holleitner, Nat. Commun. **6**, 6617 (2015).
[25] L. Prechtel, L. Song, D. Schuh, P. Ajayan, W. Wegscheider, and A. W. Holleitner, Nat. Commun. **3**, 646 (2012).
[26] H. Kataura, Y. Kumazawa, Y. Maniwa, I. Umezu, S. Suzuki, Y. Ohtsuka, and Y. Achiba, Synth. Met. **103**, 2555 (1999).
[27] O. A. Dyatlova, C. Koehler, P. Vogel, E. Malic, R. M. Jain, K. C. Tvrdy, M. S. Strano, A. Knorr, and U. Woggon, Phys. Rev. B **90**, 155402 (2014).
[28] V. Perebeinos and P. Avouris, Phys. Rev. B **74**, 121410(R) (2006).

[29] R. J. Chen, N. R. Franklin, J. Kong, J. Cao, T. W. Tombler, Y. Zhang, and H. Daia, Appl. Phys. Lett. **79**, 2258 (2001).

[30] J. Appenzeller, M. Radosavljević, J. Knoch, and P. Avouris, Phys. Rev. Lett. **92**, 048301 (2004).

[31] C. Kastl, C. Karnetzky, A. Brenneis, F. Langrieger, and A. W. Holleitner, IEEE J. Sel. Top. Quantum Electron. (2017), doi:10.1109/JSTQE.2016.2641343.

[32] K. Liu, J. Deslippe, F. Xiao, R. B. Capaz, X. Hong, S. Aloni, A. Zettl, W. Wang, X. Bai, S. G. Louie, E. Wang, and F. Wang, Nat. Nanotechnol. **7**, 325 (2012).

[33] Z. Zhong, N. M. Gabor, J. E. Sharping, A. L. Gaeta, and P. L. McEuen, Nat. Nanotechnol. **3**, 201 (2008).

[34] B. H. Son, J.-K. Park, J. T. Hong, J.-Y. Park, S. Lee, and Y. H. Ahn, ACS Nano **8**, 11361 (2014).

[35] A. Liao, Y. Zhao, and E. Pop, Phys. Rev. Lett. **101**, 256804 (2008).

[36] M. S. Purewal, B. H. Hong, A. Ravi, B. Chandra, J. Hone, and P. Kim, Phys. Rev. Lett. **98**, 186808 (2007).

[37] A. Brenneis, F. Schade, S. Drieschner, F. Heimbach, H. Karl, J. A. Garrido, and A. W. Holleitner, Sci. Rep. **6**, 35654 (2016).